Myosin-1E interacts with FAK proline-rich region 1 to induce fibronectin-type matrix

Joel B. Heim[a,1], Edwin J. Squirewell[a], Ancilla Neu[b], Georg Zocher[c], Sindhuja Sominidi-Damodaran[a], Saranya P. Wyles[a], Ekaterina Nikolova[a], Nille Behrendt[d], Ditte M. Saunte[e], Jorgen Lock-Andersen[f], Krutika S. Gaonkar[g], Huihuang Yan[g], Jann N. Sarkaria[h], Mira Krendel[i], Jan van Deursen[j,k,l], Remco Sprangers[b], Thilo Stehle[c,m], Ralph T. Böttcher[n,o], Jeong-Heon Lee[p], Tamas Ordog[p], and Alexander Meves[a,j,l,2]

[a]Department of Dermatology, Mayo Clinic, Rochester, MN 55905; [b]Max Planck Institute for Developmental Biology, 72076 Tuebingen, Germany; [c]Interfaculty Institute of Biochemistry, University of Tuebingen, 72076 Tuebingen, Germany; [d]Department of Pathology, University of Copenhagen, Roskilde Hospital, DK-4000 Roskilde, Denmark; [e]Department of Dermatology, University of Copenhagen, Roskilde Hospital, DK-4000 Roskilde, Denmark; [f]Department of Plastic Surgery, University of Copenhagen, Roskilde Hospital, DK-4000 Roskilde, Denmark; [g]Division of Biostatistics and Informatics, Department of Health Science Research, Mayo Clinic, Rochester, MN 55905; [h]Department of Radiation Oncology, Mayo Clinic, Rochester, MN 55905; [i]Cell and Developmental Biology, SUNY Upstate Medical University, Syracuse, NY 13210; [j]Department of Biochemistry and Molecular Biology, Mayo Clinic, Rochester, MN 55905; [k]Department of Pediatric and Adolescent Medicine, Mayo Clinic, Rochester, MN 55905; [l]Mayo Clinic Cancer Center, Rochester, MN 55905; [m]Vanderbilt University School of Medicine, Nashville, TN 37232; [n]Department of Molecular Medicine, Max Planck Institute for Biochemistry, 82152 Martinsried, Germany; [o]German Center for Cardiovascular Research–Munich Partner Site, 80802 Munich, Germany; and [p]Epigenomics Program, Center for Individualized Medicine, Mayo Clinic, Rochester, MN 55905

Focal adhesion kinase (FAK) is a nonreceptor tyrosine kinase involved in development and human disease, including cancer. It is currently thought that the four-point one, ezrin, radixin, moesin (FERM)–kinase domain linker, which contains autophosphorylation site tyrosine (Y) 397, is not required for in vivo FAK function until late midgestation. Here, we directly tested this hypothesis by generating mice with FAK Y397-to-phenylalanine (F) mutations in the germline. We found that Y397F embryos exhibited reduced mesodermal fibronectin (FN) and osteopontin expression and died during mesoderm development akin to FAK kinase-dead mice. We identified myosin-1E (MYO1E), an actin-dependent molecular motor, to interact directly with the FAK FERM-kinase linker and induce FAK kinase activity and Y397 phosphorylation. Active FAK in turn accumulated in the nucleus where it led to the expression of osteopontin and other FN-type matrix in both mouse embryonic fibroblasts and human melanoma. Our data support a model in which FAK Y397 autophosphorylation is required for FAK function in vivo and is positively regulated by MYO1E.

focal adhesion | myosin | fibronectin | melanoma | cancer

Focal adhesion kinase (FAK) is a nonreceptor tyrosine kinase involved in many biological processes, ranging from mesoderm development to cancer cell metastasis (1). FAK localizes to focal adhesions (2), where it becomes part of a multiprotein complex that links the extracellular matrix (ECM) to the intracellular actin cytoskeleton. FAK is also found in the nucleus, where it is believed to relay information from the cell cortex (3) and induce transcriptional changes (4). The domain architecture of FAK comprises a four-point one, ezrin, radixin, moesin (FERM) domain that is separated from a C-terminal catalytic kinase domain by the FERM-kinase linker. FAK kinase-dead (5) embryos die with mesodermal defects during late gastrulation. In contrast, mice with conditional FAK deletions in the epidermis (6) or breast epithelium (7) show resistance to carcinogenesis.

Although FAK has important biological functions, the mechanisms regulating its activity are incompletely understood. For example, it is unclear whether the FERM-kinase linker that contains autophosphorylation site tyrosine (Y) 397 is required for FAK activity in vivo (8). In its closed, inactive conformation, the FAK kinase domain is autoinhibited through interaction with the N-terminal FERM domain. Y397 is nonphosphorylated (9). Upon activation by tethering (10) or other stimuli that induce conformational change (11), the linker region is exposed and Y397 becomes autophosphorylated, leading to the recruitment of the protooncogene SRC. FAK and SRC then form a transient complex, which stabilizes FAK in its active conformation and

induces changes in cell shape and focal adhesion turnover in vitro (12). However, mice with a 19-aa deletion in the FAK linker that includes Y397 develop normally until midgestation (8).

Here, we have mechanistically discerned the contributions of Y397 to FAK function in vivo. Moreover, we screened for proteins that directly interact with the FAK linker, activate FAK kinase activity, and induce Y397 autophosphorylation.

Results

FAK Y397F Embryos Die Early During Mesoderm Development. To determine the contribution of the FAK FERM-kinase domain linker to FAK function in vivo, Y397 was substituted with the nonphosphorylatable amino acid phenylalanine (F) in the germline of mice (Fig. S1). Although mice heterozygous for the Y397F mutation displayed no apparent phenotype, their intercross failed to produce live homozygous offspring (Tables S1 and S2). Timed matings revealed that the development of homozygous FAK Y397F embryos stalled at embryonic day (E) 9.5 with a phenotype characterized by hemorrhage, an unorganized somite structure,

---

Significance

Focal adhesion kinase (FAK) is an intensely studied protein involved in many medically relevant biological processes, including cancer. Despite the large interest in FAK, a promising strategy to target FAK therapeutically is elusive. Here, we show that a region within the FAK protein that contains autophosphorylation site tyrosine (Y) 397 is essential for FAK activity in vivo. Myosin-1E (MYO1E), an actin-dependent molecular motor protein, directly interacts with FAK to induce Y397 autophosphorylation, which, in turn, causes changes in gene expression commonly observed in aggressive cancer. Our findings are significant because they further delineate FAK function in vivo and identify the MYO1E–FAK interaction as a possible Achilles' heel for cancer.

CELL BIOLOGY

and an enlarged and unfused allantois (Fig. 1*A*). Whole-mount 3D imaging of CD31-immunostained blood vessels in FAK Y397F embryos demonstrated severely malformed or absent intersomitic vessels (Fig. 1*B*) and a lack of small vascular networks (Fig. 1*C* and Movies S1 and S2). FAK Y397F yolk sacs were without differentiated blood vessels (Fig. 1*D*).

The phenotype of FAK Y397F resembled the phenotype of fibronectin (FN)-deficient embryos (13). Because FAK has been shown to mediate FN expression (14) and an FN-rich matrix is critical for angiogenesis (13), we tested whether the vascular phenotype of FAK Y397F embryos was accompanied by an abnormal FN-type matrix. We found that FN protein was substantially reduced in cryosections of E9.5 FAK Y397F embryos (Fig. 1*E*), whereas laminin and collagen expression was unchanged (Fig. 1*E*). Using quantitative PCR on whole-embryo–derived RNA at E9.5 to screen for other ECM affected by FAK Y397F, we found a strong mutation-induced reduction in the expression of osteopontin (SPP1; Fig. 1*F*), an Arg-Gly-Asp (RGD) tripeptide-containing ligand of FN-binding integrins involved in angiogenesis and bone formation (15). Together, our data showed that the FAK FERM-kinase linker is required for normal mesoderm development and the expression of FN-type ECM.

FAK Proline-Rich Region 1 Binds Myosin 1E Through Arginine 358 and Prolines 371 and 374. Next, we wanted to define the protein complex that forms at the FERM-kinase linker to promote FAK function through Y397 and induce FN-type ECM. To identify FAK linker interacting protein(s), we used stable isotope labeling by amino
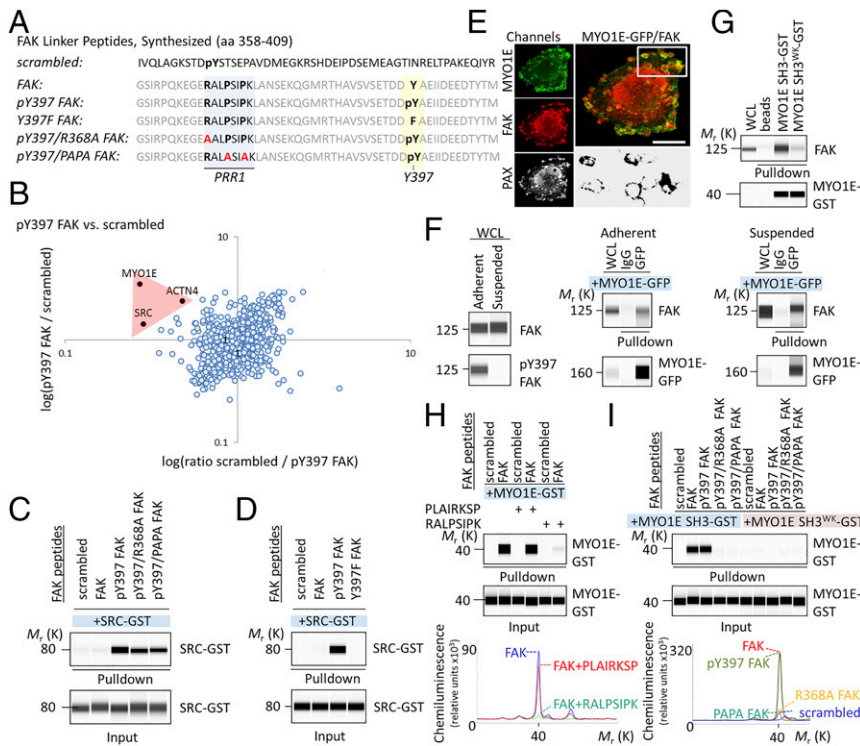
acids in cell culture (SILAC), followed by pull-down experiments with synthesized FAK linker peptide (amino acids 358–409; Fig. 2*A*) or scrambled peptide (to identify nonspecific interactors). Protein identification and quantification was by mass spectrometry-based proteomics. Among proteins that bound specifically to phospho-Y397 FAK peptide were SRC, actinin-4 (ACTN4), and myosin-1E (MYO1E) (Fig. 2*B*). Of these proteins, only MYO1E bound to nonphosphorylated FAK peptide versus scrambled peptide (Fig. S2*A*) and equally well to phospho-Y397 and nonphosphorylated FAK peptides (Fig. S2*B*). To test whether the binding of SRC, MYO1E, and ACTN4 to FAK peptides was direct or indirect, we produced GST-tagged recombinant protein and pursued in vitro binding studies. We found that recombinant GST-tagged ACTN4 did not bind FAK peptides directly. In agreement with the proteomics data, full-length SRC-GST precipitated with phospho-Y397, but not nonphosphorylated FAK peptide (Fig. 2*C*) or FAK Y397F peptide (Fig. 2*D*).

MYO1E, the third identified FAK interacting protein, is one of only two class I myosins that contain an SH3 domain (16). MYO1E has previously been shown to localize to integrin adhesions (17) and to colocalize with paxillin in cancer cell invadosomes (16), where it promotes receptor-mediated endocytosis (18). In WM858 melanoma cells, a BRAF^{V600E} cell line that expresses high amounts of FN and SPP1 (19), MYO1E organized into rosette-like structures surrounding a paxillin core (Fig. 2*E*). FAK and MYO1E colocalized in a confocal plane at the interface of the core and rosette (Fig. 2*E*). Endogenous FAK from adherent or suspended cells coimmunoprecipitated with full-length MYO1E irrespective of FAK Y397 phosphorylation (Fig. 2*F*) and was pulled down by recombinant GST-tagged wild-type MYO1E SH3, but not by mutated MYO1E SH3, harboring a tryptophan (W)-to-lysine (K) mutation at position 1088 (W1088K; Fig. 2*G*). The folding of this mutant was confirmed by circular dichroism and NMR (Fig. S3). Moreover, recombinant MYO1E SH3 bound directly to the synthesized and bead-immobilized FAK linker (amino acids 358–409; Fig. 2*H*). This interaction was almost completely disrupted by the addition of RALPSIPK (Fig. 2*H*), an octapeptide uniquely found in FAK proline-rich region 1 (PRR1) and sufficient to bind MYO1E SH3 (Fig. S4). No effects on MYO1E SH3 binding could be observed upon addition of the scrambled PLAIRKSP peptide (Fig. 2*H*). Because these findings indicated that MYO1E binds PRR1 of FAK, we next synthesized peptides with point mutations in critical PRR1 residues: mutations in arginine (R) 368, which is thought to form a salt bridge with E1070 of MYO1E, and in prolines (P) 371/374, which likely adopt a polyproline type II helical structure that interacts with the MYO1E SH3 domain. Results showed that the R368A mutation, as well as the PP371/374AA (PAPA) mutation, inhibited FAK binding to wild-type MYO1E SH3 (Fig. 2*I*).

Structural Analysis of the MYO1E SH3–FAK PRRI Interaction. We next used NMR spectroscopy and isothermal titration calorimetry (ITC) to determine the dissociation constant (K_d) of the MYO1E SH3–FAK PRR1 interaction. Recombinant ^{15}N-labeled apo MYO1E SH3 showed a very high-quality NMR spectrum with well-dispersed peaks indicating a folded and monomeric protein. Upon addition of RALPSIPK peptide, peaks affected by the interaction shifted due to changes in the environment of affected amino acids. The chemical shift perturbations (CSPs) of four peaks observed during titration were used to determine the K_d of the interaction at 51 μM (Fig. 3*A*). The K_d determined by NMR was then used to define the setup of two independent ITC experiments, which yielded a K_d of 22 ± 1 μM (Fig. 3*B*), confirming the order of magnitude of the affinity of this interaction. These affinities were similar to the affinities of the SRC SH3–FAK PRR1 interaction with reported K_ds between 32 and 63 μM depending on method (20). To investigate the mode of interaction between FAK PRR1 and MYO1E SH3, we assigned the peaks in the ^{1}H^{15}N spectrum; we then quantified the CSPs and mapped them on the structure of human MYO1E SH3 [Protein
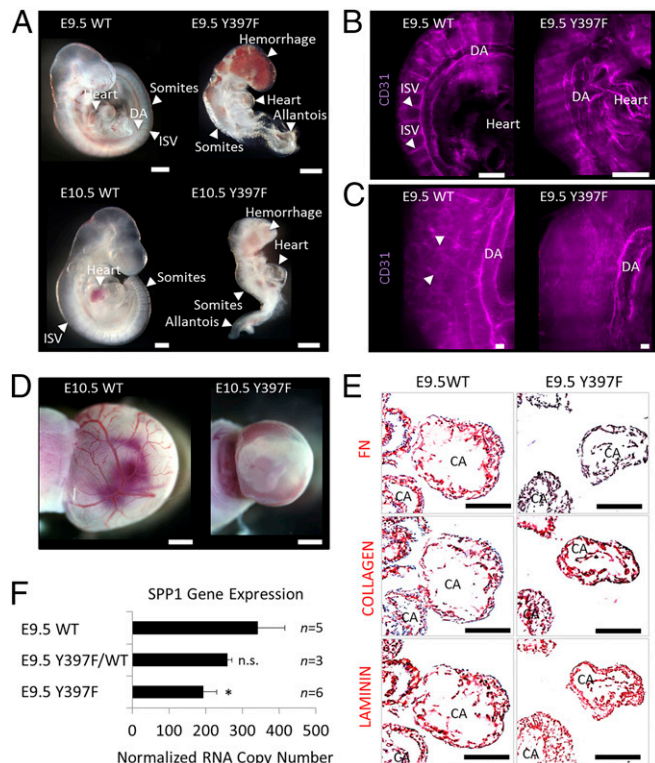
Fig. 1. FAK Y397F mutation is early embryonic lethal. (*A*) Bright-field images of E9.5 and E10.5 wild-type (WT) and Y397F embryos. DA, dorsal aorta; ISV, intersomitic vessel. (*B*) Whole-mount pictures of E9.5 WT and Y397F embryos stained for CD31 (purple). (*C*) Higher magnification of CD31-stained vasculature. Arrowheads point to a web of small vessels in WT embryos. (*D*) E10.5 control and Y397F yolk sacs. (*E*) Immunohistochemistry staining of E9.5 embryo frozen sections using the indicated antibodies. CA, cardiac mesoderm. (*F*) SPP1 RNA copy numbers as determined by quantitative PCR in E9.5 whole-embryo–derived RNA. *P = 0.002, Student's *t* test. n.s., not significant. (Scale bars, 200 μm.)

A FAK Linker Peptides, Synthesized (aa 358-409)

scrambled:	IVQLAGKSTD**pY**STSEPAVDMEGKRSHDEIPDSEMEAGTINRELTPAKEQIYR
FAK:	GSIRPQKEGE**RALPSIPK**LANSEKQGMRTHAVSVSETDD Y AEIIDEEDTYTM
pY397 FAK:	GSIRPQKEGE**RALPSIPK**LANSEKQGMRTHAVSVSETDD**pY**AEIIDEEDTYTM
Y397F FAK:	GSIRPQKEGE**RALPSIPK**LANSEKQGMRTHAVSVSETDD F AEIIDEEDTYTM
pY397/R368A FAK:	GSIRPQKEGE**AALPSIPK**LANSEKQGMRTHAVSVSETDD**pY**AEIIDEEDTYTM
pY397/PAPA FAK:	GSIRPQKEGE**RALASIAK**LANSEKQGMRTHAVSVSETDD**pY**AEIIDEEDTYTM
	PRR1 _____ Y397

Fig. 2. MYO1E binds FAK at PRR1. (*A*) Amino acid (aa) sequence of synthesized FAK peptides. (*B*) Scatter plot of phospho-Y397 FAK peptide versus scrambled peptide pull-down results. The log SILAC ratio of proteins identified with at least two unique peptides in each mass spectrometry run is plotted as the forward pull-down (*x* axis) against the reverse labeling pull-down (*y* axis). Specific interaction partners show inverse ratios between forward and reverse experiments, grouping them into the upper left quadrant. (*C* and *D*) Pull-down of recombinant SRC-GST by FAK peptides. (*E*) Immunostaining of MYO1E-GFP–expressing WM858 cells. (*Lower Right*) Area of MYO1E/FAK colocalization. (Scale bars, 10 μm.) (*F*) Coimmunoprecipitation of FAK by MYO1E-GFP from whole-cell lysates (WCL) of adherent or suspended WM858 cells. (*G*) Pull-down assay demonstrating MYO1E SH3 binding to FAK. A tryptophan (W) to lysine (K) mutation at position 1088 (W1088K; WK) in MYO1E SH3 prevented MYO1E SH3 binding to FAK. (*H*) FAK PRR1 peptide RALPSIPK, but not scrambled PLAIRKSP, blocks FAK interaction with MYO1E SH3. Chemiluminescence spectra for the indicated pull-downs are shown. (*I*) Pull-down of recombinant MYO1E SH3-GST by FAK peptides. Chemiluminescence spectra are shown. Immunoblots are pseudoimages generated by ProteinSimple Compass software.

Data Bank (PDB) ID code 2XMF] (Fig. 3*C*). Although CSPs are spread throughout the domain, the part of the protein most affected by the binding clusters to one region, exemplified by the strong shifts in residues W1089, F1100, N1102, and N1103. Additionally, we assigned the peaks corresponding to the side chain imines of W1088 and W1089 (Fig. S3*B*), and found that the side chain of the crucial residue, W1088, displays a very large CSP, even though the perturbation of the backbone amide is only moderate. This binding surface is in accordance with the canonical binding surface of proline-rich peptides on SH3 domains, located in-between the RT loop and the n-Src loop on the C-terminal helix. Superposition of the MYO1E SH3 domain with the structure of the SRC SH3 domain in complex with a class 1 peptide confirms this mode of interaction. This model underlines the importance of peptide residues R368, P371, and P374 for the interactions that were observed in pull-down experiments.

Myosin 1E Induces FAK Kinase Activity and Downstream SPP1 Expression in Fibroblasts. To test whether MYO1E SH3 induces FAK kinase activity, we performed in vitro FAK kinase reactions in the presence of 1:2 titrated MYO1E SH3. When MYO1E SH3 was incubated with full-length FAK, kinase activity increased several fold (Fig. 4*A*). An increase in kinase activity was not observed when MYO1E SH3 was incubated with FAK kinase domain (amino acids 393–698) devoid of FAK PRR1 (Fig. 4*A*). To test whether FAK PRR1 induces FAK Y397 autophosphorylation in cells, we reconstituted FAK-null fibroblasts with PRR1-mutated FAK. Immunoblots revealed a significant reduction in phospho-Y397 FAK with the PAPA or R368A mutation. When separating nuclear from cytoplasmic fractions, R368A or PAPA-induced reductions in phospho-Y397 FAK were in the nuclear compartment (Fig. 4*B*). Conversely, reexpression of MYO1E in MYO1E-null fibroblasts increased FAK Y397 phosphorylation (Fig. 4*C*). Specifically, MYO1E promoted the nuclear accumulation of total and phospho-Y397 FAK (Fig. 4*D*).

Because phospho-Y397 FAK was abundant in the nucleus of MYO1E-reconstituted cells, we next tested whether FAK Y397 promoted the expression of FN-type ECM as observed in FAK Y397F embryos. Total sequencing of RNA from FAK-null

or FAK-reconstituted wild-type or Y397F fibroblasts yielded ~41,000 sequenced genes. Two hundred seventy-two genes were in a union of genes differentially expressed in FAK-null versus wild-type fibroblasts and FAK wild-type versus Y397F fibroblasts (Dataset S1). One hundred one genes had lower expression in FAK-null and Y397F cells compared with FAK wild-type cells, and thus depended on Y397 for their up-regulation; functional association analysis of these 101 genes by STRING (string-db.org) revealed an FN-centered cluster (Fig. 4*E*). One of the most highly FAK-induced genes was SPP1 (Fig. 4*F*). In line with these data, reexpression of MYO1E in MYO1E-null fibroblasts induced SPP1/FN mRNA (Fig. 4*G*), whereas SPP1/FN mRNA was reduced in the presence of FAK PAPA compared with wild-type FAK (Fig. 4*H*). Consistent with the role of FN and SPP1 in promoting cell proliferation and invasion, FAK Y397F fibroblasts grew less confluently and invaded less well into Matrigel than wild-type controls (Fig. 4*I*). Likewise, FAK PAPA fibroblasts grew less confluently than wild-type controls (Fig. 4*J*). Conversely, MYO1E-reconstituted fibroblasts grew more confluently and invaded faster into Matrigel than MYO1E-null controls (Fig. 4*K*).

MYO1E/FAK Induces SPP1 Promoter Activity and Proliferation in Melanoma Cells. FAK and MYO1E could be visualized in the cytoplasm and nucleus of WM858 melanoma cells by postembedding immunogold electron microscopy (Fig. 5*A*). In these SPP1/FN high-expressing cancer cells (19), the nuclear-to-cytoplasmic phospho-Y397 FAK ratio was high (Fig. 5*B*) compared with wild-type FAK-cherry reconstituted mouse embryonic fibroblasts (Fig. 5*C*). High levels of nuclear phospho-Y397 FAK were also observed in patient-derived melanoma xenograft cell lines M12 and M15 and patient-derived in-transit cutaneous melanoma metastases (Fig. S5). To test whether Y397 phosphorylation promotes FAK nuclear accumulation, WM858 cells were treated with the FAK kinase inhibitor PF-562271, which prevented FAK Y397 phosphorylation. We found that nuclear FAK was reduced in the presence of PF-562271, as was nuclear SRC (Fig. 5*B*). Moreover, in WM858 cells that expressed wild-type or Y397F FAK-cherry, nuclear Y397F was

CELL BIOLOGY
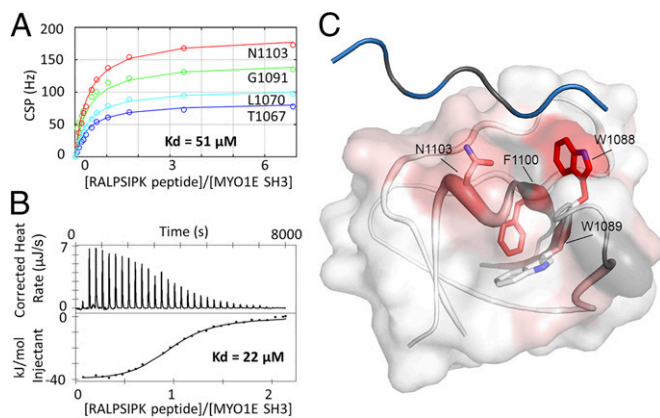
Fig. 3. Structural analysis of the RALPSIPK–MYO1E interaction. (*A*) Quantification of CSPs as determined by NMR during peptide titration based on four resonances (L1070, G1091, N1003, and T1067). The combined fit yields an affinity of $K_d = 51 \mu M$. (*B*) ITC experiment of MYO1E SH3 with RALPSIPK peptide. The experimental K_d determined by ITC is $22 \pm 1 \mu M$ with thermodynamic parameters of dH = −43.0 ± 2.2 kJ/mol ($n = 0.94 \pm 0.02$) and dS = −55 ± 8 J/(mol * K). (*C*) CSPs on MYO1E SH3 upon binding of RALPSIPK peptide and modeled class 1 peptide. CSPs are mapped on the crystal structure of MYO1E SH3 (PDB ID code 2XMF). Increasing color and diameter of the cartoon indicate higher CSP of the corresponding backbone amide. Additionally, the CSP of the tryptophane imides is depicted as the color of the surface representation. Prolines are depicted in gray because they do not appear in the NMR $^1H^{15}N$ spectra. The position of the depicted class 1 peptide is derived from the structure of chicken SRC SH3 domain in complex with a proline-rich peptide by superimposing the MYO1E SH3 with the chicken SRC SH3 domain (PDB ID code 1RLQ).

reduced compared with wild type (Fig. 5*F*), indicating that the Y397F mutation interferes with nuclear FAK accumulation. Likewise, total and phospho-Y397 nuclear FAK was reduced in cells with reduced MYO1E mRNA due to effective MYO1E shRNA derived from RNAi Consortium (TRC) clones 152421 and 152890 versus ineffective shRNA from clone 151296 and nontargeting control shRNA (Fig. 5*G*).

To investigate whether nuclear FAK promotes FN-type ECM expression in WM858 cells, we performed six chromatin immuno-precipitation with massively parallel DNA sequencing (ChIP-seq) experiments. These experiments revealed that FAK associates with the consensus binding sequence GCGC[AC]TGCGC. This binding sequence is highly similar to the optimal binding site for nuclear respiratory factor 1 (NRF1), (T/C)GCGCA(C/T)GCGC(A/G) (Fig. S6), which coregulates promoter activity of SPP1 family genes (21). To test whether FAK drives SPP1 promoter activity, we tagged the endogenous SPP1 promoter in WM858 cells with a dual-luciferase reporter (Dual-Glo cells). Firefly luciferase was introduced to assay SPP1 promoter activity, and Renilla luciferase was coupled to the CMV promoter as a loading control. As expected, the SPP1 promoter was activated by vitamin D, because it was shown to harbor vitamin D response elements (22) (Fig. 5*H*). Retinoic acid receptor agonists, reported previously to induce SPP1 (23), also induced SPP1 promoter activity (Fig. 5*I*), as did stable overexpression of FAK wild type-cherry and MYO1E-GFP (Fig. 5*J*). We then performed an unbiased screen of pharmaceutically active compounds to identify compounds that inhibit SPP1 promoter activity. We found that the structurally related FAK kinase inhibitors PF-431396 and PF-562271 were among a handful of drugs that strongly inhibited SPP1 promoter activity (Fig. 5*K*). Another structurally unrelated FAK inhibitor, PF-573228, was less potent. Interestingly, neither SRC kinase inhibitors nor small-molecule inhibitors of mitogen-activated or rapidly accelerated fibrosarcoma kinases (RAFs) inhibited SPP1 promoter activity (Fig. S7).

SPP1 promotes melanoma cell proliferation and tumor growth (24). Exposure of WM858 or M12 cells to PF-562271 inhibited proliferation, as determined by automated counting of fluorescently labeled nuclei with a half-maximal effective concentration of 0.3 ± 0.1 μM. Likewise, isopropyl β-D-1-thiogalactopyranoside–inducible shRNA targeting FAK in WM858 cells inhibited proliferation (Fig. 5*L*). When FAK-depleted cells were transiently reconstituted with either wild-type or PAPA mutant murine FAK, wild-type cells proliferated faster (Fig. 5*M*). Moreover, knockdown of MYO1E using effective shRNA TRCN152890, but not ineffective shRNA TRCN151296 or nontargeting control shRNA, inhibited proliferation of WM858 cells (Fig. 5*N*). Together, these data are consistent with a model where upon MYO1E interaction with FAK in melanoma cells, FAK becomes activated and accumulates in the nucleus to induce SPP1 promoter activity and proliferation. In line
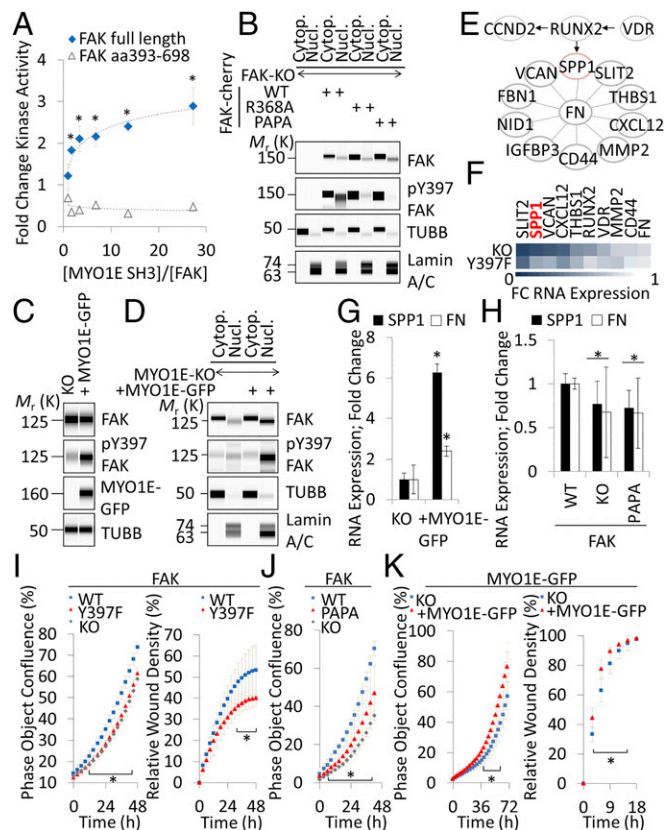
Fig. 4. MYO1E activates FAK to induce SPP1 expression in fibroblasts. (*A*) In vitro FAK kinase activity of full-length recombinant FAK versus FAK kinase domain only (aa 393–698) in the presence or absence of 1:2 titrated recombinant MYO1E SH3 (mean ± SEM, $n = 4$; *$P < 0.05$ versus no MYO1E SH3). (*B*) Effects of FAK PRR1 mutations on nuclear (Nucl.) and cytoplasmic (Cytop.) FAK in transiently transfected fibroblasts. (*C*) Immunodetection of the indicated antigens in stably MYO1E-GFP–reconstituted MYO1E-null mouse embryonic fibroblasts. (*D*) Nuclear versus cytoplasmic localization of FAK in MYO1E-null (KO) or WT MYO1E-GFP–reconstituted fibroblasts. (*E*) Network of differentially regulated FN-associated genes. Arrows and lines indicate a functional relationship as determined by STRING. (*F*) Color-coded ratios of mRNA expression as quantified by RNA sequencing in FAK-null (KO) or Y397F-reconstituted fibroblasts over WT. FC, fold change. RNA expression of the indicated genes in MYO1E-null (KO) or WT MYO1E-GFP–reconstituted fibroblasts (*G*) or FAK-null fibroblasts transiently reconstituted with WT or PAPA FAK (*H*) is shown. Gene expression was determined by quantitative PCR (mean ± SD, $n \geq 4$; *$P < 0.05$). (*I*–*K*) Phase object confluence or Matrigel invasion of the indicated reconstituted and nonreconstituted KO fibroblasts (mean ± SD, $n = 4$; *$P < 0.05$, Student's *t* test). Immunoblots are pseudoimages generated by ProteinSimple Compass software.
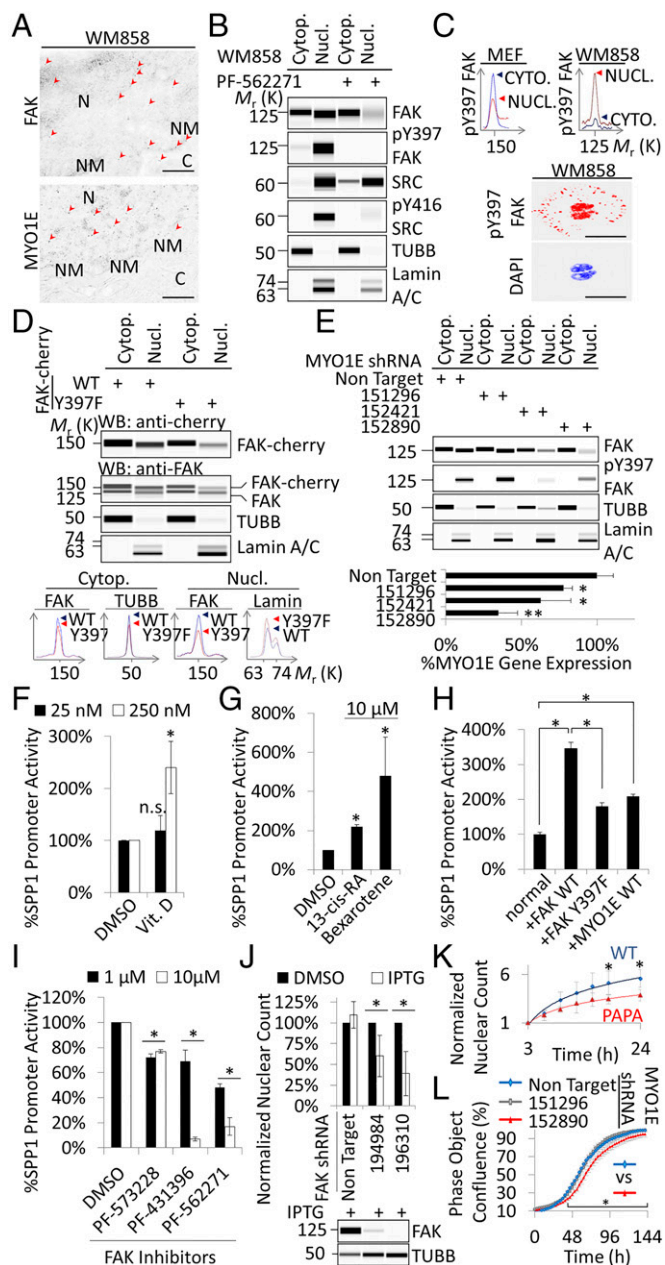
Fig. 5. MYO1E/FAK drives SPP1 expression and proliferation in melanoma cells. (*A*) Immunogold electron microscopy micrographs of WM858 cells. Arrowheads point to areas of electron-dense immunolabeling. C, cytoplasm; N, nucleus; NM, nuclear membrane. (Scale bar, 0.5 μm.) (*B*) Analysis of nuclear and cytoplasmic protein extracts from WM858 cells in the presence or absence of 2.5 μM PF-562271. (*C*, *Top*) Phospho-Y397 FAK chemiluminescence spectra of fractionated lysates of the indicated cell types. MEF, mouse embryonic fibroblast. (*C*, *Bottom*) WM858 cell stained for phospho-Y397. Note high levels of phospho-Y397 FAK in the nucleus. (Scale bars, 40 μm.) (*D*) Analysis of nuclear and cytoplasmic protein extracts from WM858 cells carrying stable WT or Y397F FAK-cherry. Chemiluminescence spectra for the indicated subcellular fractions, antibodies, and cells are shown. WB, Western blot. (*E*) Effects of MYO1E shRNA-mediated knockdowns on FAK levels in WM858 cells. Knockdown efficacy was determined by quantitative PCR (mean ± SD, n = 3; *P < 0.05, **P < 0.001 versus nontargeting shRNA). SPP1 promoter activity after overnight exposure of Dual-Glo cells to vitamin (Vit.) D (*F*) or retinoids (*G*) is shown (mean ± SD, n = 3; *P < 0.05). n.s., not significant. (*H*) SPP1 promoter activity in normal (unmodified) Dual-Glo cells or cells with stable expression of the indicated FAK or MYO1E constructs (mean ± SD, n = 16; *P < 0.001). (*I*) SPP1 promoter activity after exposure of Dual-Glo cells to FAK inhibitors (mean ± SD, n = 3; *P < 0.05). (*J*) Proliferation of WM858 cells as determined by automated

counting of fluorescent nuclei in the presence or absence of shRNA targeting FAK, inducible by isopropyl β-D-1-thiogalactopyranoside (IPTG) (mean ± SD, n = 3; *P < 0.05). TUBB, β-tubulin. (*K*) Proliferation of WM858 cells depleted of endogenous FAK by shRNA TRCN196310 and transiently reconstituted with murine FAK-cherry (mean ± SD, n ≥ 3; *P < 0.05). (*L*) Proliferation of WM858 cells in the presence or absence of MYO1E shRNA (mean ± SEM, n = 12; *P < 0.05). Immunoblots are pseudoimages generated by ProteinSimple Compass software.

with this model, nuclear phospho-Y397 FAK–positive cutaneous melanoma expressed higher levels of SPP1 than nuclear phospho-Y397 FAK–negative precursor tissue (Fig. S5). Moreover, in cutaneous melanoma, mitotic rate is an independent adverse predictor of survival (25), indicating a possible role for MYO1E/FAK-driven cancer cell proliferation in prognostically important processes.

Discussion

In the present study, we found that FAK function in vivo critically depends on the release of FAK kinase autoinhibition and dependent Y397 autophosphorylation. Moreover, FAK kinase activity is induced by a direct interaction of MYO1E and FAK. Once the FAK kinase domain is released from autoinhibition, SRC binds to phospho-Y397, thereby stabilizing the release of autoinhibition (9). Full catalytic activity in turn leads to nuclear accumulation of FAK, and transcription of FAK target genes such as SPP1 and FN.

We identified MYO1E as a FAK PRR1 interactor. In contrast to SRC, MYO1E binds the FERM-kinase linker in the absence of phospho-Y397. MYO1E SH3-mediated autoinhibition of MYO1E motor function (26) may be released by MYO1E binding to FAK. MYO1E binding to FAK then tethers FAK to actin, which may promote endocytosis (18) and could explain why FAK function is tightly linked to actomyosin dynamics and integrin endocytosis (10, 27). Upon FAK Y397 autophosphorylation, SRC binds FAK through SH2 domain interaction, which, in turn, releases SRC SH3 to interact with FAK PRR1, thereby possibly replacing MYO1E. Simultaneous binding of SRC SH2 and SH3 to FAK linker profoundly increases affinity versus SH2 binding alone (20). In the absence of phospho-Y397, the affinity of MYO1E SH3 for FAK PRR1 octapeptide RALPSIPK is only marginally higher than the affinity of SRC SH3. However, in peptide pull-down experiments using full-length nonphosphorylated FAK linker peptide, SRC is not easily precipitated (via its SH3 domain) in the absence of Y397 phosphorylation. This finding suggests that the affinity of full-length SRC for FAK linker is lower than the affinity of recombinant SRC SH3 (28), specifically in the absence of SH2 binding to phospho-Y397, or that MYO1E and FAK interact at additional sites outside of the RALPSIPK sequence either directly or indirectly that have yet to be determined.

The ability of MYO1E/FAK to influence matrix composition is consistent with in vivo MYO1E/FAK mutant phenotypes. Normal epidermis, which is avascular and does not depend on FN receptors and ligands, is unaffected by changes in MYO1E or FAK function (6, 29). On the other hand, complex mesenchymal processes such as neovascularization require the induction of an FN-based ECM (30) and are affected by FAK (31) or MYO1E loss of function (29). Cancer cells produce an FN-rich fibrotic matrix to facilitate metastasis, and both FAK (4, 7) and MYO1E (32) promote carcinogenesis in murine cancer models. In addition, MYO1E protects kidney podocytes from mechanical stress-induced injury, as does SPP1, which may be induced by FAK (33, 34). Moreover, keloid formation (i.e., a wound-healing reaction with excessive scar formation) has been associated with MYO1E (35) and FAK function (36). MYO1E/FAK-induced SPP1 may play a role in keloid formation because SPP1 is known to drive tissue fibrosis (37).

CELL BIOLOGY

Melanoma expresses high levels of SPP1 and other FN-type ECM, which, in turn, promotes metastasis (19, 38). Consistent with a role of nuclear phospho-Y397 FAK in driving SPP1 expression, we found high levels of phospho-Y397 FAK in the nucleus of patient-derived melanoma tissues and cell lines. In mouse embryonic fibroblasts, phospho-Y397 FAK was abundant in the cytoplasm. Other authors have reported a predominantly cytoplasmic localization of phospho-Y397 FAK [e.g., in human umbilical vein endothelial cells (3)]. The molecular basis for this discrepancy is not well understood but may involve MYO1E. Future research must address the mechanisms that drive the nuclear shuttling of FAK to provide additional insight into medically relevant processes that rely on ECM remodeling.

Materials and Methods

Patient Material, Mouse Work, and Cell Lines. All animal studies were approved by the Institutional Animal Care and Use Committee at the Mayo Clinic. Patient studies were approved by the Mayo Foundation Institutional Review Board. A consent waiver was obtained based on US Department of Health and Human Services regulations. Details on plasmids, constructs, cell lines, transient and stable transfection/transduction techniques, timed matings, embryo isolation, whole-mount 3D imaging of embryos, quantitative microfluidic PCR, gene expression by RNA sequencing, proliferation and Matrigel invasion assays, immunocytochemistry, immunohistochemistry, ChIP-seq, and FAK kinase assays are provided in *SI Materials and Methods*.

Pharmaceutically Active Compounds and Antibodies. Details on drugs and antibodies are provided in *SI Materials and Methods*.

SILAC-Based Peptide Pull-Downs. SILAC labeling of WM858 melanoma cells was by $^{13}C_6$ L-lysine and $^{13}C_6$, $^{15}N_4$ L-arginine. Proteins were precipitated as described previously (39).

NMR Spectroscopy. NMR spectra were recorded at 25 °C on a Bruker AVIII-600 spectrometer with a room temperature probe head. Details on NMR and the expression and purification of recombinant proteins are provided in *SI Materials and Methods*.

ITC. Binding constants were determined using a NanoITC instrument (TA Instruments). Details are provided in *SI Materials and Methods*.

Nuclear Extractions. Separation of the nuclear fraction from the cytoplasmic fraction of cells was achieved using a kit (40010; Active Motif) and following the manufacturer's instructions. Details on coimmunoprecipitation, GST pull-downs, and microfluidic Western blots by ProteinSimple are provided in *SI Materials and Methods*.

Statistics. Statistical analysis was performed using GraphPad Prism software (version 6.05; GraphPad Software). Statistical significance was determined as indicated.

1. Ilić D, et al. (1995) Reduced cell motility and enhanced focal adhesion contact formation in cells from FAK-deficient mice. *Nature* 377:539–544.
2. Schiller HB, Friedel CC, Boulegue C, Fässler R (2011) Quantitative proteomics of the integrin adhesome show a myosin II-dependent recruitment of LIM domain proteins. *EMBO Rep* 12:259–266.
3. Lim ST, et al. (2008) Nuclear FAK promotes cell proliferation and survival through FERM-enhanced p53 degradation. *Mol Cell* 29:9–22.
4. Serrels A, et al. (2015) Nuclear FAK controls chemokine transcription, Tregs, and evasion of anti-tumor immunity. *Cell* 163:160–173.
5. Lim ST, et al. (2010) Knock-in mutation reveals an essential role for focal adhesion kinase activity in blood vessel morphogenesis and cell motility-polarity but not cell proliferation. *J Biol Chem* 285:21526–21536.
6. McLean GW, et al. (2004) Specific deletion of focal adhesion kinase suppresses tumor formation and blocks malignant progression. *Genes Dev* 18:2998–3003.
7. Lahlou H, et al. (2007) Mammary epithelial-specific disruption of the focal adhesion kinase blocks mammary tumor progression. *Proc Natl Acad Sci USA* 104:20302–20307.
8. Corsi JM, et al. (2009) Autophosphorylation-independent and -dependent functions of focal adhesion kinase during development. *J Biol Chem* 284:34769–34776.
9. Lietha D, et al. (2007) Structural basis for the autoinhibition of focal adhesion kinase. *Cell* 129:1177–1187.
10. Shi Q, Boettiger D (2003) A novel mode for integrin-mediated signaling: Tethering is required for phosphorylation of FAK Y397. *Mol Biol Cell* 14:4306–4315.
11. Cai X, et al. (2008) Spatial and temporal regulation of focal adhesion kinase activity in living cells. *Mol Cell Biol* 28:201–214.
12. Mitra SK, Hanson DA, Schlaepfer DD (2005) Focal adhesion kinase: in command and control of cell motility. *Nat Rev Mol Cell Biol* 6:56–68.
13. George EL, Georges-Labouesse EN, Patel-King RS, Rayburn H, Hynes RO (1993) Defects in mesoderm, neural tube and vascular development in mouse embryos lacking fibronectin. *Development* 119:1079–1091.
14. Cicchini C, et al. (2008) TGFbeta-induced EMT requires focal adhesion kinase (FAK) signaling. *Exp Cell Res* 314:143–152.
15. Duvall CL, Taylor WR, Weiss D, Wojtowicz AM, Guldberg RE (2007) Impaired angiogenesis, early callus formation, and late stage remodeling in fracture healing of osteopontin-deficient mice. *J Bone Miner Res* 22:286–297.
16. Ouderkirk JL, Krendel M (2014) Myosin 1e is a component of the invadosome core that contributes to regulation of invadosome dynamics. *Exp Cell Res* 322:265–276.
17. Schiller HB, Fässler R (2013) Mechanosensitivity and compositional dynamics of cell-matrix adhesions. *EMBO Rep* 14:509–519.
18. Krendel M, Osterweil EK, Mooseker MS (2007) Myosin 1E interacts with synaptojanin-1 and dynamin and is involved in endocytosis. *FEBS Lett* 581:644–650.
19. Hoek KS, et al. (2006) Metastatic potential of melanomas defined by specific gene expression profiles with no BRAF signature. *Pigment Cell Res* 19:290–302.
20. Thomas JW, et al. (1998) SH2- and SH3-mediated interactions between focal adhesion kinase and Src. *J Biol Chem* 273:577–583.
21. Narayanan K, et al. (2004) The CCAAT enhancer-binding protein (C/EBP)β and Nrf1 interact to regulate dentin sialophosphoprotein (DSPP) gene expression during odontoblast differentiation. *J Biol Chem* 279:45423–45432.
22. Noda M, et al. (1990) Identification of a DNA sequence responsible for binding of the 1,25-dihydroxyvitamin D3 receptor and 1,25-dihydroxyvitamin D3 enhancement of mouse secreted phosphoprotein 1 (SPP-1 or osteopontin) gene expression. *Proc Natl Acad Sci USA* 87:9995–9999.
23. Kaji H, et al. (1995) Retinoic acid induces osteoclast-like cell formation by directly acting on hemopoietic blast cells and stimulates osteopontin mRNA expression in isolated osteoclasts. *Life Sci* 56:1903–1913.
24. Philip S, Bulbule A, Kundu GC (2001) Osteopontin stimulates tumor growth and activation of promatrix metalloproteinase-2 through nuclear factor-κ B-mediated induction of membrane type 1 matrix metalloproteinase in murine melanoma cells. *J Biol Chem* 276:44926–44935.
25. Thompson JF, et al. (2011) Prognostic significance of mitotic rate in localized primary cutaneous melanoma: An analysis of patients in the multi-institutional American Joint Committee on Cancer melanoma staging database. *J Clin Oncol* 29:2199–2205.
26. Stöffler H-E, Bähler M (1998) The ATPase activity of Myr3, a rat myosin I, is allosterically inhibited by its own tail domain and by Ca2+ binding to its light chain calmodulin. *J Biol Chem* 273:14605–14611.
27. De Franceschi N, et al. (2016) Selective integrin endocytosis is driven by interactions between the integrin α-chain and AP2. *Nat Struct Mol Biol* 23:172–179.
28. Xu W, Doshi A, Lei M, Eck MJ, Harrison SC (1999) Crystal structures of c-Src reveal features of its autoinhibitory mechanism. *Mol Cell* 3:629–638.
29. Krendel M, et al. (2009) Disruption of Myosin 1e promotes podocyte injury. *J Am Soc Nephrol* 20:86–94.
30. Zhou X, et al. (2008) Fibronectin fibrillogenesis regulates three-dimensional neovessel formation. *Genes Dev* 22:1231–1243.
31. Furuta Y, et al. (1995) Mesodermal defect in late phase of gastrulation by a targeted mutation of focal adhesion kinase, FAK. *Oncogene* 11:1989–1995.
32. Ouderkirk-Pecone JL, et al. (2016) Myosin 1e promotes breast cancer malignancy by enhancing tumor cell proliferation and stimulating tumor cell de-differentiation. *Oncotarget* 7:46419–46432.
33. Endlich N, et al. (2002) Analysis of differential gene expression in stretched podocytes: Osteopontin enhances adaptation of podocytes to mechanical stress. *FASEB J* 16:1850–1852.
34. Mele C, et al.; PodoNet Consortium (2011) MYO1E mutations and childhood familial focal segmental glomerulosclerosis. *N Engl J Med* 365:295–306.
35. Velez Edwards DR, Tsosie KS, Williams SM, Edwards TL, Russell SB (2014) Admixture mapping identifies a locus at 15q21.2-22.3 associated with keloid formation in African Americans. *Hum Genet* 133:1513–1523.
36. Wong VW, et al. (2011) Focal adhesion kinase links mechanical force to skin fibrosis via inflammatory signaling. *Nat Med* 18:148–152.
37. Mori R, Shaw TJ, Martin P (2008) Molecular mechanisms linking wound inflammation and fibrosis: Knockdown of osteopontin leads to rapid repair and reduced scarring. *J Exp Med* 205:43–51.
38. Meves A, et al. (2015) Tumor Cell adhesion as a risk factor for sentinel lymph node metastasis in primary cutaneous melanoma. *J Clin Oncol* 33:2509–2515.
39. Meves A, et al. (2011) Beta1 integrin cytoplasmic tyrosines promote skin tumorigenesis independent of their phosphorylation. *Proc Natl Acad Sci USA* 108:15213–15218.
40. Yokomizo T, et al. (2012) Whole-mount three-dimensional imaging of internally localized immunostained cells within mouse embryos. *Nat Protoc* 7:421–431.